Supplementary Information for:
Suppressing parasitic flow in membraneless diffusion-based microfluidic gradient generators

Vahid Khandan,[a] Ryan C. Chiechi, [b,c] Elisabeth Verpoorte[a] and Klaus Mathwig*[a,d]

[a] *University of Groningen Groningen Research Institute of Pharmacy, Pharmaceutical Analysis, 9700 AD Groningen, the Netherlands*

[b] *Stratingh Institute for Chemistry and Zernike Institute for Advanced Materials, University of Groningen, Nijenborgh 4, 9747 AG Groningen, the Netherlands*

[c] *Department of Chemistry & Organic and Carbon Electronics Laboratory, North Carolina State University, Raleigh, NC, 27695 USA*

[d] *imec within OnePlanet Research Center, Bronland 10, 6708 WH Wageningen, the Netherlands* klaus.mathwig@imec.nl

Accelerated gradient response of a membraneless DMGGs

As illustrated in Figure S1, diffusion-based microfluidic gradient generators (DMGGs) typically incorporate a permeable membrane to suppress parasitic flow within the gradient region. While the membrane effectively minimizes parasitic flow, its presence introduces a delay in gradient formation due to the reduced diffusion rate across the membrane's porous structure. In this study, we propose the removal of the permeable membrane as a strategy to accelerate gradient formation.

To demonstrate this effect, we conducted a series of COMSOL simulations to investigate how membrane porosity impacts the diffusion process and slows down the establishment of the concentration gradient within the mixing microchannel. These simulations employed "*Transport of Diluted Species in Porous Media*" interface to model the time-dependent evolution of the concentration gradient $c(x,y,t)$ within a two-dimensional (2D) mixing microchannel shown in Figure S1. The microchannel has a length of $L = 200\,\mu m$ and a width of $W = 10\,\mu m$, with an integrated membrane of thickness $t_m = 10\,\mu m$. The boundary conditions were set to maintain a high concentration $C_H = 10\,mM$ at one end and a low concentration $C_L = 0$ at the opposite end. The initial concentration across the microchannel was uniformly set to $c(x,y,t=0) = C_L$, ensuring a well-defined starting condition for diffusion. Additionally, the Bruggeman model was applied to account for membrane tortuosity, accurately reflecting the reduction in diffusivity caused by membrane porosity.

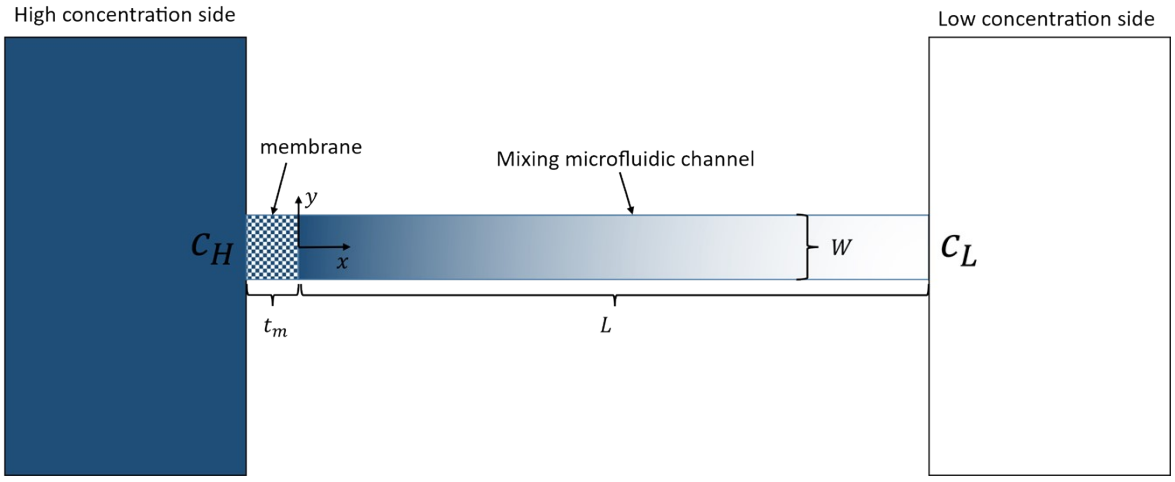

Figure S1. A two-dimensional schematic of a microchannel (dimensions: width W × height L) incorporating a membrane of thickness t_m to suppress parasitic flow. The established concentration gradient across the channel is visually represented using a blue-white colormap, where blue indicates the high concentration region (C_H) and white represents the low concentration region (C_L). These concentrations are precisely maintained by large side access channels positioned on the left and right sides of the microchannel, ensuring a steady boundary condition.

The simulation results for two solutes with diffusivities of $D = 10^{-9} m^2/s$ and $D = 10^{-10} m^2/s$ are presented in Figure S2. These results compare the effects of different membrane porosities, with values of $Pr = 0.1$ and $Pr = 0.5$, as well as the membraneless condition represented by $Pr = 1$. To quantify the evolution of the concentration gradient over time, the parameter $\varepsilon(t)$ is introduced, which describes the progression of the two-dimensional gradient profile and is expressed as

$$\varepsilon(t) = \frac{\int_0^W \int_0^L \left| c(x,y,t) - c_\infty(x,y) \right| dxdy}{WL}, \qquad \text{Equation S1}$$

where, $c_\infty(x,y) = c(x,y,t_\infty)$ represents the steady-state concentration gradient established at the end of the time-dependent simulation. The steady-state time is defined as $t_\infty = 60\ s$ and $t_\infty = 600\ s$ for $D = 10^{-9} m^2/s$ and $D = 10^{-10} m^2/s$, respectively. This steady-state time is significantly longer than the time required for the concentration gradient to stabilize, which is influenced by the preset membrane porosity. To better capture the impact of membrane porosity on gradient formation, an additional parameter, termed relaxation time (t_r), is introduced. The relaxation time is defined as the moment when the gradient profile evolution parameter reaches a threshold value of $\varepsilon(t_r) = 0.1\ mM$. This metric provides a more practical assessment of the gradient formation dynamics, offering insights into how membrane porosity affects the speed at which the system reaches an equilibrium state.

As demonstrated in Figure S2, membranes with higher porosity exhibit greater initial variations in the gradient profile evolution, $\varepsilon(t)$, during the early stages of gradient formation. This behavior is attributed to the lower tortuosity of highly porous membranes, which imposes less resistance to diffusion, allowing solutes to traverse the membrane more efficiently. As a result, the system achieves equilibrium more rapidly, as indicated by the shorter relaxation time observed in membranes with higher porosity.

The results confirm that removing the permeable membrane significantly accelerates gradient formation by eliminating diffusion resistance and allowing solutes to disperse more rapidly within the microchannel. However, this approach makes DMGGs more susceptible to parasitic flow, which can disrupt the gradient stability and uniformity. To address this challenge, we have introduced novel H-

junction and Y-junction designs, which effectively mitigate parasitic flow while maintaining the accelerated gradient formation.

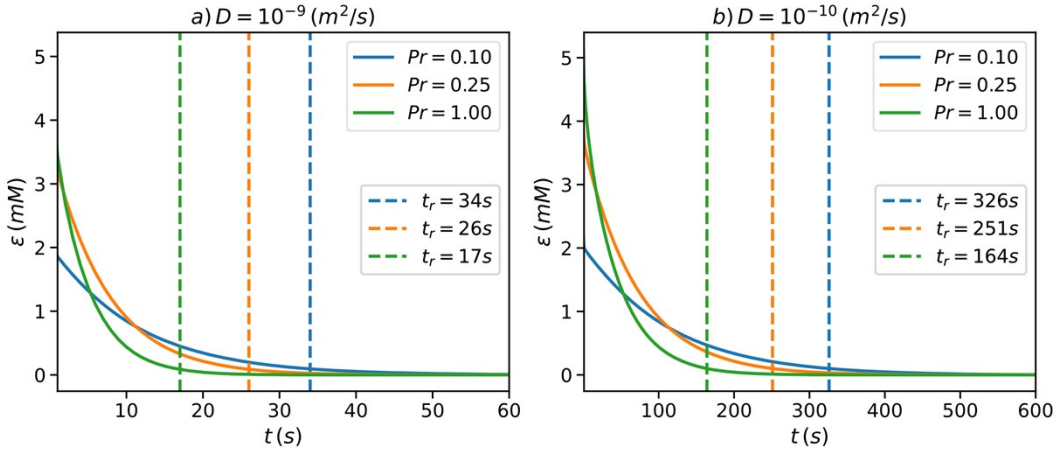

Figure S2. Time-dependent simulation results of concentration gradient formation in the mixing microchannel (illustrated in Figure S1) for two solutes with diffusivities of (**a**) $D = 10^{-9} m^2/s$ and (**b**) $D = 10^{-10} m^2/s$. The gradient profile evolution, $\varepsilon(t)$, is calculated from the simulated time-dependent concentration distribution, $c(x,y,t)$, using Equation S1, based on the applied boundary conditions $c(x = 0,y,t) = 10\,mM$ and $c(x = L,y,t) = 0$, with an initial condition of $c(x,y,t = 0) = 0$. The results demonstrate that membranes with higher porosity facilitate faster equilibrium by offering lower resistance to diffusion, as reflected by the shorter relaxation time.

Expanded Finite Element Simulation Results

The results presented in the *Finite Element Simulation* section are expanded here to illustrate the generated parasitic flow corresponding to the parasitic flow velocities shown in Figs. 5d, 5e, and 5f of the main manuscript.

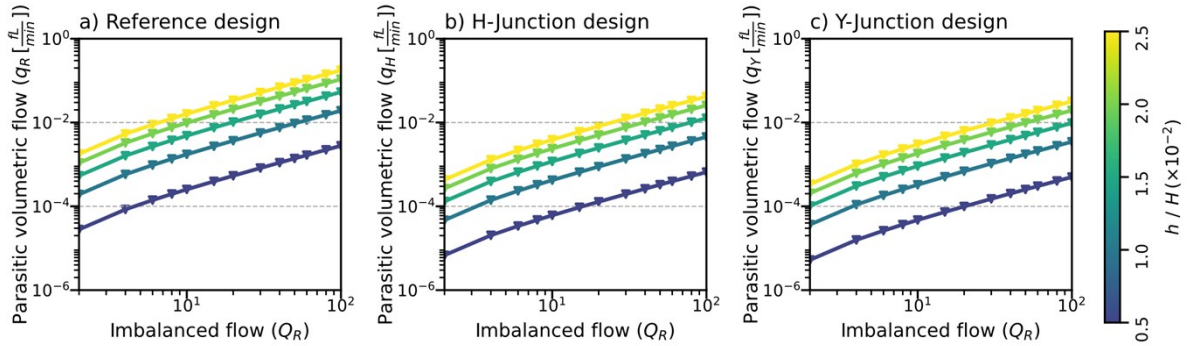

Figure S3. Parasitic flow induced by imbalanced flow conditions ($Q_R \neq 1$) in the Reference (a), H-junction (b), and Y-junction (c) designs at varying height ratios $\frac{h}{H}$.

Particle Image Velocimetry

A video is provided to complement the results of Particle Image Velocimetry (PIV) analysis illustrated in Fig. 6 in the main paper.

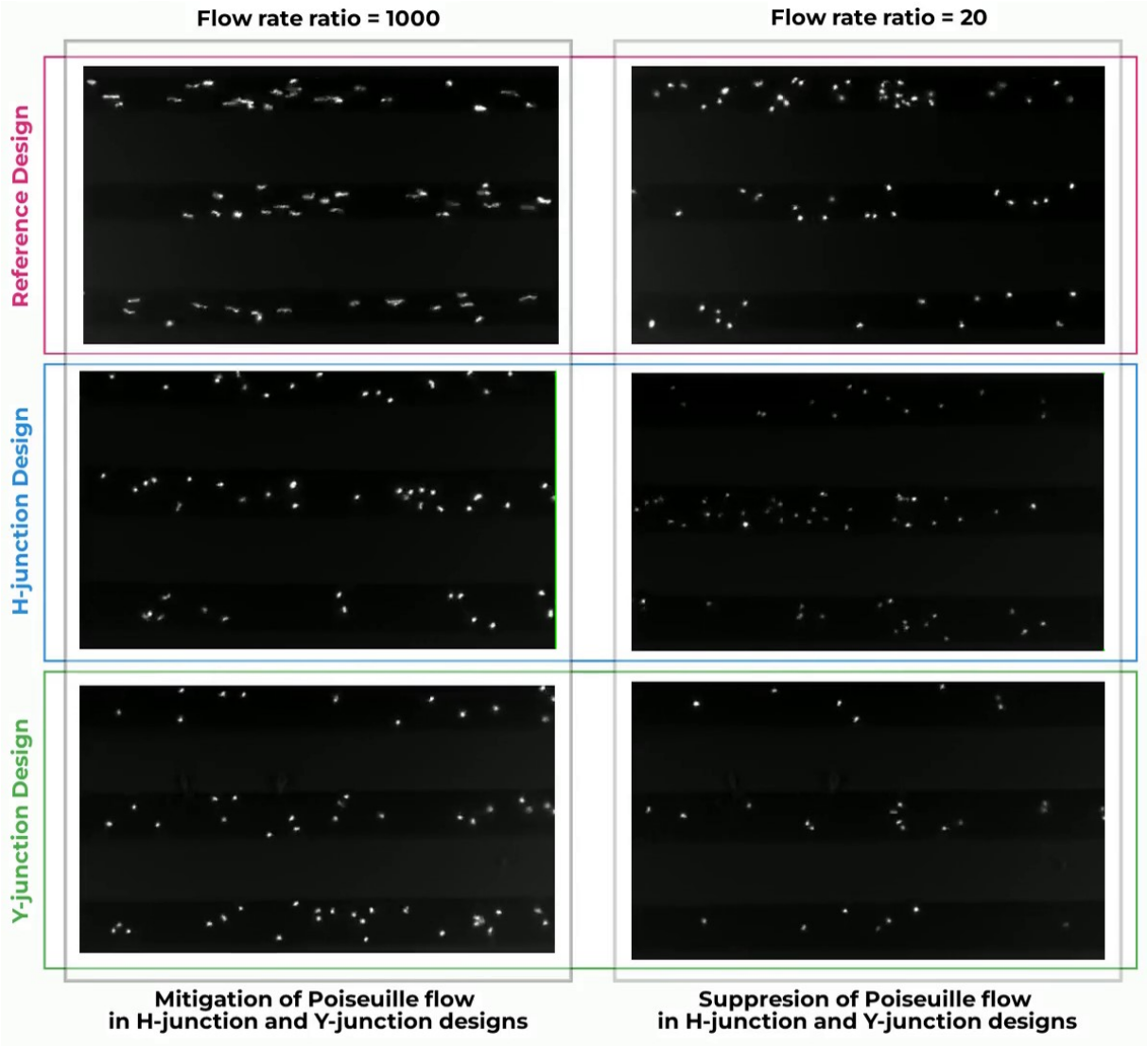

Video S1. Mitigation and suppression of parasitic flow within the microchannel using the H-junction and Y-junction designs. Polystyrene nanoparticles with a diameter of 200 nm suspended in Milli-Q water at a concentration of 50 $\mu g/ml$ were introduced into both the left and right side-channels at constant flow rates of Q_L and Q_H, respectively. In all experiments, Q_L is consistently set to 5 $\mu L/h$. Depending on their column location (highlighted in light grey), the experiments have different Q_H settings: those in the left column have a Q_H of 5000 $\mu L/h$, resulting in a flow rate ratio Q_R of 1000, whereas those in the right column have a Q_H of 100 $\mu L/h$, yielding a Q_R of 20. As visually demonstrated, the parasitic flow generated in the Reference design is substantially more pronounced than that in the H-junction and Y-junction designs when a flow rate ratio Q_R of 1000 is applied (as indicated in the left column). Furthermore, at a lower flow rate ratio of $Q_R = 20$, parasitic flow is nearly undetectable in the H-junction and Y-junction designs, whereas it remains clearly visible in the Reference design.

Link to video: https://figshare.com/s/b81d49897570ce9a3e1e